



Contents lists available at ScienceDirect

## Commun Nonlinear Sci Numer Simulat

journal homepage: [www.elsevier.com/locate/cnsns](http://www.elsevier.com/locate/cnsns)

# A model-coupling framework for nearshore waves, currents, sediment transport, and seabed morphology

H.S. Tang<sup>a,\*</sup>, T.R. Keen<sup>b</sup>, R. Khanbilvardi<sup>a</sup><sup>a</sup> Dept. of Civil Eng., City College, City University of New York, 138th Street and Convent Ave., New York, NY 10031, USA<sup>b</sup> Oceanography Div., Code 7320, Naval Research Laboratory, Stennis Space Center, MS 39529, USA

## ARTICLE INFO

## Article history:

Received 16 October 2008

Accepted 16 October 2008

Available online 30 October 2008

## PACS:

02.60.Cb

02.70.Bf

91.50.Cw

91.50.Ga

92.10.Hm

92.10.A–

## Keywords:

Wave

Current

Sediment transport

Seabed morphology

Model coupling

## ABSTRACT

This paper presents a framework for synchronously coupling wave, current, sediment transport, and seabed morphology for the accurate simulation of multi-physics coastal ocean processes. The governing equations, which represent models that are commonly adopted in practical simulations, are discretized using finite-difference methods. The resulting system is validated against analytical solutions. In order to test the performance of the proposed framework and the numerical methods, dam-break flow over a mobile-bed and evolution of a wave-driven sand dune are simulated. The interactions among waves, currents, and seabed morphology are illustrated.

© 2008 Elsevier B.V. All rights reserved.

## 1. Introduction

Nearshore hydrodynamics has a direct impact on societal issues such as coastal engineering, environmental protection, recreation, and military operations (e.g., [1,2]). Wave, current, sediment transport, and morphology are important processes within coastal and estuarine settings, and consequently a number of models have been developed to simulate and predict their behaviors in the past few decades. For example, models have been designed to forecast global currents, salinity, sea level, temperature, and turbulence distributions (e.g., [3,4]) and nearshore wave-driven currents (e.g., [5]). In addition, a number of models have been designed to simulate surface wave propagation (e.g., [6,7]). Models have also been proposed to predict sediment transport and seabed morphology (e.g., [8,9]).

Since actual coastal ocean flows are multi-physical processes with complex interactions among hydrodynamic, sediment transport, and morphological phenomena, the consideration of feedback between these individual physical phenomena is necessary to accurately simulate the flows. Model coupling has been implemented for the prediction of many actual problems; for instance, a wave model has been incorporated into a primitive-equation model to study wave-current interaction [10]. This study demonstrated that decoupling currents and waves leads to inaccurate water elevation prediction. Wave and

\* Corresponding author. Tel.: +1 212 650 8006; fax: +1 212 650 6965.

E-mail addresses: [htang@ce.cuny.cuny.edu](mailto:htang@ce.cuny.cuny.edu) (H.S. Tang), [tim.keen@nrlssc.navy.mil](mailto:tim.keen@nrlssc.navy.mil) (T.R. Keen), [rk@ce.cuny.cuny.edu](mailto:rk@ce.cuny.cuny.edu) (R. Khanbilvardi).

<sup>1</sup> Previously at Oceanography Div., Code 7320, Naval Research Laboratory, Stennis Space Center, MS 39529, USA.

morphology models have been added into the Delft Hydraulics model (DELFT3D) (e.g., [9]). Efforts have also been made to couple the Simulating WAVes Nearshore (SWAN) model with a current model to simulate sediment transport (e.g., [11]). Nevertheless, strictly speaking, until now the coupling between currents, waves, sediment transport, and morphology has been non-synchronic or merely partially implemented. For example, the wave computation is not simultaneously carried out with that for currents and morphology in simulations described in [9]; also, in coupling of SWAN with the Advanced Circulation (ADCIRC) model [12], the wave component is updated only once in solving the current and sediment transport equations.

In order to understand complex phenomena within coastal ocean flows, it is necessary to fully couple waves, current, and sediment transport/seabed morphology. To this end, a number of investigations have been made on numerical methods for such coupling. Rogers et al. [13] designed a Godunov-type method, together with an adaptive grid scheme, to simultaneously simulate ray-type wave–current interaction. Murillo et al. [14] combined inviscid shallow water and solute equations into a single system and proposed a finite volume method based on the Roe average. Hudson and Sweby [15,16] made a systematic study of different formulations to couple currents and morphology. Rosatti and Fraccarollo [17] constructed a Godunov scheme for currents over a mobile-bed. An important issue is discretization of the source terms in the coupling systems (e.g., [18]). A so-called C-property is proposed to enforce balance between numerical fluxes and non-homogeneous source terms in cases of steady flows (e.g., [19]). Nevertheless, in previous investigations, the coupling has been usually between two or, occasionally, three components among wave, current, sediment transport, and morphological processes.

In order to accurately take their interactions into account, this paper presents a framework to synchronously couple wave, current, sediment transport, and morphological processes. This coupled system consists of governing equations that reproduce typical models used for both research and engineering problems. The wave action equation is used for wave propagation. The shallow water equations are employed to describe currents and storm surge. Sediment transport is described by a convection–diffusion equation. Morphology evolution is depicted by the Exner equation. In this paper, all of these equations are discretized using common schemes, which advance in time synchronously, or with same time steps. The resulting system is validated using analytical solutions. In order to demonstrate the performance of the framework, simulations are presented of dam-break flow over a mobile-bed and wave-driven flow over a sand dune.

The paper is organized as follows. Section 2 presents the coupled system with governing equations for waves, currents, sediment transport, and morphology, together with a discussion on their coupling. Section 3 deals with discretization of the system. Section 4 discusses validation of the system and two example simulations. Section 5 concludes the paper.

## 2. Governing equations

The governing equation for wave action is given in a conservation form as (e.g., [20])

$$\frac{\partial N}{\partial t} + \frac{\partial C_{gx}N}{\partial x} + \frac{\partial C_{gy}N}{\partial y} + \frac{\partial C_{\sigma}N}{\partial \sigma} + \frac{\partial C_{\theta}N}{\partial \theta} = S, \quad (1)$$

where  $t$  is the time,  $x$  and  $y$  are the Cartesian coordinates,  $\sigma$  is the frequency, and  $\theta$  is the angle of the wave propagation direction.  $N$  is the wave action,  $C_{gx}$  and  $C_{gy}$  are respectively the wave speed in  $x$ - and  $y$ -direction in the physical space  $(x, y)$ ,  $C_{\sigma}$  and  $C_{\theta}$  are respectively wave speed in  $\sigma$ - and  $\theta$ -direction in the spectrum space  $(\sigma, \theta)$ .  $S$  is a source term that represents the combined effects of wind and other processes. Using linear wave theory, it has been shown for short waves that (e.g., [20])

$$C_{gx} = \frac{g}{2\sigma} \cos \theta + U, \quad (2a)$$

$$C_{gy} = \frac{g}{2\sigma} \sin \theta + V, \quad (2b)$$

$$C_{\sigma} = -\frac{\sigma}{2} \left( \frac{\partial U}{\partial x} \cos^2 \theta + \left( \frac{\partial U}{\partial y} + \frac{\partial V}{\partial x} \right) \sin \theta \cos \theta + \frac{\partial V}{\partial y} \sin^2 \theta \right), \quad (2c)$$

$$C_{\theta} = -\frac{\partial U}{\partial y} \cos^2 \theta + \left( \frac{\partial U}{\partial x} - \frac{\partial V}{\partial y} \right) \sin \theta \cos \theta + \frac{\partial V}{\partial x} \sin^2 \theta, \quad (2d)$$

and for long waves that

$$C_{gx} = \sqrt{gH} \cos \theta + U, \quad (3a)$$

$$C_{gy} = \sqrt{gH} \sin \theta + V, \quad (3b)$$

$$C_{\sigma} = -\frac{\sigma}{2} \left( \frac{\partial U}{\partial x} + \frac{\partial V}{\partial y} \right) - \sigma \left( \frac{\partial U}{\partial x} \cos^2 \theta + \left( \frac{\partial U}{\partial y} + \frac{\partial V}{\partial x} \right) \sin \theta \cos \theta + \frac{\partial V}{\partial y} \sin^2 \theta \right), \quad (3c)$$

$$C_{\theta} = \frac{\sigma}{2H} \left( \frac{\partial H}{\partial x} \sin \theta - \frac{\partial H}{\partial y} \cos \theta \right) - \frac{\partial U}{\partial y} \cos^2 \theta + \left( \frac{\partial U}{\partial x} - \frac{\partial V}{\partial y} \right) \sin \theta \cos \theta + \frac{\partial V}{\partial x} \sin^2 \theta. \quad (3d)$$

In the above,  $U$  and  $V$  are the current velocities in  $x$ - and  $y$ -directions, respectively,  $H$  is the water depth, and  $g$  is the gravity constant. For convenience in computation, only short and long wave situations are considered here. Short waves are defined as those with  $kH > \pi$ , and long waves as those with  $kH < \pi/10$ . Here  $k$  is the wave number. For further details, readers are referred to [20,21].

The shallow water equations consist of the equation of mass conservation (e.g., [20])

$$\frac{\partial H}{\partial t} + \frac{\partial HU}{\partial x} + \frac{\partial HV}{\partial y} = 0, \tag{4a}$$

and the equations of momentum conservation

$$\frac{\partial HU}{\partial t} + \frac{\partial HU^2}{\partial x} + \frac{\partial HUV}{\partial y} = -gH \frac{\partial \eta}{\partial x} + \frac{\partial}{\partial x} \left( 2\nu_t H \frac{\partial U}{\partial x} \right) + \frac{\partial}{\partial y} \left( \nu_t H \left( \frac{\partial U}{\partial y} + \frac{\partial V}{\partial x} \right) \right) + \frac{\tau_x^s - \tau_x^b}{\rho} - \frac{1}{\rho} \left( \frac{\partial S_{xx}}{\partial x} + \frac{\partial S_{xy}}{\partial y} \right), \tag{4b}$$

$$\frac{\partial HV}{\partial t} + \frac{\partial HUV}{\partial x} + \frac{\partial HV^2}{\partial y} = -gH \frac{\partial \eta}{\partial y} + \frac{\partial}{\partial x} \left( \nu_t H \left( \frac{\partial U}{\partial y} + \frac{\partial V}{\partial x} \right) \right) + \frac{\partial}{\partial y} \left( 2\nu_t H \frac{\partial V}{\partial y} \right) + \frac{\tau_y^s - \tau_y^b}{\rho} - \frac{1}{\rho} \left( \frac{\partial S_{yx}}{\partial x} + \frac{\partial S_{yy}}{\partial y} \right), \tag{4c}$$

where  $\nu_t$  is the turbulence eddy viscosity, and  $\rho$  is the density.  $\eta$  is the water surface elevation,  $\tau_x^s$  and  $\tau_y^s$  are the surface friction stresses in  $x$ - and  $y$ -directions, respectively, and  $\tau_x^b$  and  $\tau_y^b$  are the bottom friction stresses in  $x$ - and  $y$ -directions, respectively.  $S_{xx}$ ,  $S_{xy}$ , and  $S_{yy}$  are the radiation stresses resulting from waves. It is readily seen that, for the case of a flat bottom,  $H\partial\eta/\partial x = \partial(H^2/2)/\partial x$  and  $H\partial\eta/\partial y = \partial(H^2/2)/\partial y$ , and the shallow water equations will be in conservation forms with the friction stresses as source terms.

The turbulence eddy viscosity is calculated as follows (e.g., [22,23]):

$$\nu_t = \alpha_t g n^2 H^{2/3} \sqrt{U^2 + V^2}, \tag{5}$$

where  $\alpha_t$  is a constant ranging from 0.3 to 1,  $n$  is the Manning friction coefficient. It is proposed to treat wave effects on bottom friction as follows (e.g., [24]):

$$\tau_x^b = \rho g n^2 H^{-1/3} U \sqrt{U^2 + V^2} + \frac{1}{2} \rho f_w U_w^2, \quad \tau_y^b = \rho g n^2 H^{-1/3} V \sqrt{U^2 + V^2} + \frac{1}{2} \rho f_w U_w^2, \tag{6}$$

where  $U_w = A\sigma/\sin h(kH)$ , the near-bed wave orbit velocity, and  $f_w$  is the wave friction factor. Here,  $A$  is the wave amplitude. In the case of short waves,  $kH \gg 1$  and  $\sigma = \sqrt{gk}$ , thus  $U_w \approx 0$ , and

$$\tau_x^b = \rho g n^2 H^{-1/3} U \sqrt{U^2 + V^2}, \quad \tau_y^b = \rho g n^2 H^{-1/3} V \sqrt{U^2 + V^2}. \tag{7a}$$

In the case of long waves,  $kH \ll 1$  and  $\sigma = k\sqrt{gH}$ , thus  $U_w \approx A\sqrt{g/H}$ . Since  $E = \rho g A^2/2$  ( $E$  is the wave density and it equals  $N/\sigma$ ),  $U_w \approx \sqrt{2N/\rho\sigma H}$ . As a result, one has

$$\tau_x^b = \rho g n^2 H^{-1/3} U \sqrt{U^2 + V^2} + \frac{f_w N}{\sigma H}, \quad \tau_y^b = \rho g n^2 H^{-1/3} V \sqrt{U^2 + V^2} + \frac{f_w N}{\sigma H}. \tag{7b}$$

For the surface stress, a widely used formula is (e.g., [25,26])

$$\tau_x^s = C_D \rho_{air} W_x W, \quad \tau_y^s = C_D \rho_{air} W_y W, \tag{8a}$$

where  $W_x$  and  $W_y$  are wind speed in  $x$ - and  $y$ -directions, respectively,  $W$  is the total wind speed,  $W = \sqrt{W_x^2 + W_y^2}$ ,  $\rho_{air}$  is the air density, and the drag coefficient is given as

$$C_D = \begin{cases} 1.2875 \times 10^{-3}, & W \leq 7.5 \text{ m/s}, \\ (0.8 + 0.065W) \times 10^{-3}, & W > 7.5 \text{ m/s}. \end{cases} \tag{8b}$$

Assuming linear wave theory, the radiation stresses for short waves are given as (e.g., [20])

$$S_{xx} = \frac{g}{2} \iint N \cos^2 \theta \, d\sigma d\theta, \tag{9a}$$

$$S_{xy} = S_{yx} = \frac{g}{2} \iint N \sin \theta \cos \theta \, d\sigma d\theta, \tag{9b}$$

$$S_{yy} = \frac{g}{2} \iint N \sin^2 \theta \, d\sigma d\theta, \tag{9c}$$

and for long waves,

$$S_{xx} = g \iint N(\cos^2 \theta + 0.5) \, d\sigma d\theta, \tag{10a}$$

$$S_{xy} = S_{yx} = g \iint N \sin \theta \cos \theta \, d\sigma d\theta, \tag{10b}$$

$$S_{yy} = g \iint N(\sin^2 \theta + 0.5) \, d\sigma d\theta. \tag{10c}$$

The sediment transport equation is a convection–diffusion equation with a source term, for which the conservation form is (e.g., [22])

$$\frac{\partial HC}{\partial t} + \frac{\partial HUC}{\partial x} + \frac{\partial HVC}{\partial y} = D_c \left( \frac{\partial^2 HC}{\partial x^2} + \frac{\partial^2 HC}{\partial y^2} \right) - \alpha\omega(C - C_*), \tag{11}$$

where  $C$  is the concentration for sediment,  $C^*$  is the sediment concentration under equilibrium conditions,  $D_c$  is the diffusivity coefficient,  $\alpha$  is the coefficient of suspended load, and  $\omega$  is the settling velocity. The seabed morphology is controlled by the Exner equation (e.g., [27,28]):

$$\frac{\partial H_b}{\partial t} + \frac{\partial BU(U^2 + V^2)^q}{\partial x} + \frac{\partial BV(U^2 + V^2)^q}{\partial y} = 0. \tag{12}$$

Here  $H_b$  is the elevation of the seabed, and  $B$  and  $q$  are constants. Typically,  $B$  depends on flow velocity, water depth, sediment grain sizes, and other factors, and  $q$  is usually in the range of  $0.5 \leq q \leq 1.5$ ,  $\eta = H + H_b$ . In this paper,  $q = 1$  is used.

Eqs. (1), (4), (11) and (12) comprise a coupled non-homogeneous system of conservation laws, which reproduces the framework of well-known models. Eqs. (1) and (4) can be viewed as a result of flow decomposition in the Navier–Stokes equations (e.g., [20]). The wave action Eq. (1) is employed in models such as in SWAN [6]. The shallow water Eqs. (4) are used for models such as SHORECIRC [5]. The sediment transport Eq. (11) and morphology evolution Eq. (12) are also widely employed in engineering (e.g., [22,29]).

The interactions among wave, current, sediment transport, and morphology can be seen in the system equations; in Eqs. (2) the wave field is coupled with the current through the velocity,  $U$  and  $V$ . As indicated in Eqs. (4) the current is affected by the wave field through the radiation and bottom stresses,  $S_{xy}$ ,  $S_{yy}$  and  $\tau_x^b$ ,  $\tau_y^b$ , respectively, and by sediment transport and morphology evolution through turbulence eddy viscosity  $\nu_t$  and bottom elevation  $H_b$ . Both sediment transport and morphology are directly related to the current through the velocity field as shown in Eqs. (11) and (12). It should be noted that, as seen in Eqs. (2) because wave action occurs in spectral space as well as physical space, each term on the right hand side of Eq. (1) is coupled with the current through the velocity field. Furthermore, sediment concentration and morphology are directly related to each other (e.g., [22]). In this paper, however, in view that their governing Eqs. (11) and (12) have different unknowns, which are sediment concentration and bed elevation, sediment transport and morphology are indirectly coupled through the velocity field.

### 3. Numerical methods

The coupled system of waves, currents, sediment transport, and morphology are discretized as follows. For wave action Eq. (1), the following first-order accurate extension of the one-dimensional Lax–Friedrich scheme [30] is used:

$$N_i^{n+1} = \frac{1}{8} \sum_{i',j',k',l'=-1,1} N_{i+i',j+j',k+k',l+l'}^n - \frac{\Delta t}{2} D_i(C_{gx}N)_{ij,k,l}^n - \frac{\Delta t}{2} D_j(C_{gy}N)_{ij,k,l}^n - \frac{\Delta t}{2} D_k(C_{\sigma}N)_{ij,k,l}^n - \frac{\Delta t}{2} D_l(C_{\theta}N)_{ij,k,l}^n + \Delta t \left( \frac{S}{\sigma} \right)_{ij,k,l}^n, \tag{13}$$

where  $\Delta t$  is the time step,  $D_m$  is the central difference operator with respect to the  $m$ -direction ( $m = ij,k,l$ ). For instance,  $D_i(\cdot)_{ij,k,l} = ((\cdot)_{i+1,j,k,l} - (\cdot)_{i-1,j,k,l}) / (2\Delta x)$ ,  $\Delta x$  being the grid spacing in the  $x$ -direction. The shallow water Eqs. (4) and the sediment transport Eq. (11) are solved using the following MacCormack scheme [31]:

$$H_{ij}^* = H_{ij}^n - \Delta t D_i-(HU)_{ij}^n - \Delta t D_j-(HV)_{ij}^n, \tag{14a}$$

$$(HU)_{ij}^* = (HU)_{ij}^n - \Delta t D_i-(HU^2)_{ij}^n - \Delta t D_j-(HUV)_{ij}^n - g\Delta t H_{i-1/2,j}^n D_i-(H + H_b)_{ij}^n + 2\Delta t D_{i+}((v_t H)_{i-1/2,j}^n D_i-U_{ij}^n) + \Delta t D_{j+}((v_t H)_{ij-1/2}^n D_j-U_{ij}^n) + \Delta t D_j((v_t H)_{ij}^n D_i V_{ij}^n) + \frac{\Delta t(\tau_{xij}^s - \tau_{xij}^b)}{\rho} - \frac{\Delta t}{\rho} D_{i-} S_{xxij}^n - \frac{\Delta t}{\rho} D_{j-} S_{xyij}^n, \tag{14b}$$

$$(HV)_{ij}^* = (HV)_{ij}^n - \Delta t D_i-(HUV)_{ij}^n - \Delta t D_j-(HV^2)_{ij}^n - g\Delta t H_{i-1/2,j}^n D_j-(H + H_b)_{ij}^n + \Delta t D_i((v_t H)_{ij}^n D_j U_{ij}^n) + \Delta t D_{i+}((v_t H)_{i-1/2,j}^n D_i-V_{ij}^n) + 2\Delta t D_{j+}((v_t H)_{ij-1/2}^n D_j^2-V_{ij}^n) + \frac{\Delta t(\tau_{yij}^s - \tau_{yij}^b)}{\rho} - \frac{\Delta t}{\rho} D_{i-} S_{xyij}^n - \frac{\Delta t}{\rho} D_{j-} S_{yyij}^n, \tag{14c}$$

and

$$H_{ij}^{n+1} = \frac{1}{2}(H_{ij}^n + H_{ij}^*) - \frac{\Delta t}{2} D_{i+}(HU)_{ij}^* - \frac{\Delta t}{2} D_{j+}(HV)_{ij}^*, \tag{14d}$$

$$(HU)_{ij}^{n+1} = \frac{1}{2}((HU)_{ij}^n + (HU)_{ij}^*) - \frac{\Delta t}{2} D_{i+}(HU^2)_{ij}^* - \frac{\Delta t}{2} D_{j+}(HUV)_{ij}^* - \frac{g\Delta t}{2} H_{i+1/2,j}^* D_{i+}(H + H_b)_{ij}^* + \Delta t D_{i+}((v_t H)_{i-1/2,j}^* D_i-U_{ij}^*) + \frac{\Delta t}{2} D_{j+}((v_t H)_{ij-1/2}^* D_j-U_{ij}^*) + \frac{\Delta t}{2} D_j((v_t H)_{ij}^* D_i V_{ij}^*) + \frac{\Delta t(\tau_{xij}^s - \tau_{xij}^b)}{2\rho} - \frac{\Delta t}{2\rho} D_{i+} S_{xxij}^* - \frac{\Delta t}{2\rho} D_{j+} S_{xyij}^*, \tag{14e}$$

$$\begin{aligned}
 (HV)_{ij}^{n+1} = & \frac{1}{2} \left( (HV)_{ij}^n + (HV)_{ij}^* \right) - \frac{\Delta t}{2} D_{i+} (HUV)_{ij}^* - \frac{\Delta t}{2} D_{j+} (HV^2)_{ij}^* - \frac{g\Delta t}{2} H_{i+1/2}^* D_{j+} (H + H_b)_{ij}^* \\
 & + \frac{\Delta t}{2} D_i \left( (v_t H)_{ij}^* D_j U_{ij}^* \right) + \frac{\Delta t}{2} D_{i+} \left( (v_t H)_{i-1/2j}^* D_i V_{ij}^* \right) + \Delta t D_{j+} \left( (v_t H)_{ij-1/2}^* D_j V_{ij}^* \right) \\
 & + \frac{\Delta t (\tau_{yij}^{s*} - \tau_{yij}^{b*})}{2\rho} - \frac{\Delta t}{2\rho} D_{i-} S_{xyij}^* - \frac{\Delta t}{2\rho} D_{j-} S_{yyij}^*.
 \end{aligned} \tag{14f}$$

$$(HC)_{ij}^* = (HC)_{ij}^n - \Delta t D_{i-} (HUC)_{ij}^n - \Delta t D_{j-} (HVC)_{ij}^n + \Delta t D_{i+} (D_{i-} (HC)_{ij}^n) + \Delta t D_{j+} (D_{j-} (HC)_{ij}^n), \tag{15a}$$

$$(HC)_{ij}^{n+1} = \frac{1}{2} \left( (HC)_{ij}^n + (HC)_{ij}^* \right) - \frac{\Delta t}{2} D_{i+} (HUC)_{ij}^* - \frac{\Delta t}{2} D_{j+} (HVC)_{ij}^* - \frac{\Delta t}{2} D_{i+} (D_{i-} (HC)_{ij}^*) - \frac{\Delta t}{2} D_{j+} (D_{j-} (HC)_{ij}^*). \tag{15b}$$

In the above,  $D_{m-}(\cdot)_{ij}$  and  $D_{m+}(\cdot)_{ij}$  ( $m = i, j, k, l$ ) are backward and forward differences, respectively. The values at half nodes are evaluated using an arithmetic average. For example,  $(\cdot)_{i+1/2j} = ((\cdot)_{ij} + (\cdot)_{i+1j})/2$ . The morphology Eq. (12) is discretized using the following scheme:

$$H_{bij}^{n+1} = H_{bij}^n - B\Delta t D_i [U(U^2 + V^2)]_{ij}^n - B\Delta t D_j [V(U^2 + V^2)]_{ij}^n. \tag{16}$$

The time steps for integrating the wave, current, and sediment transport/morphology equations are, respectively

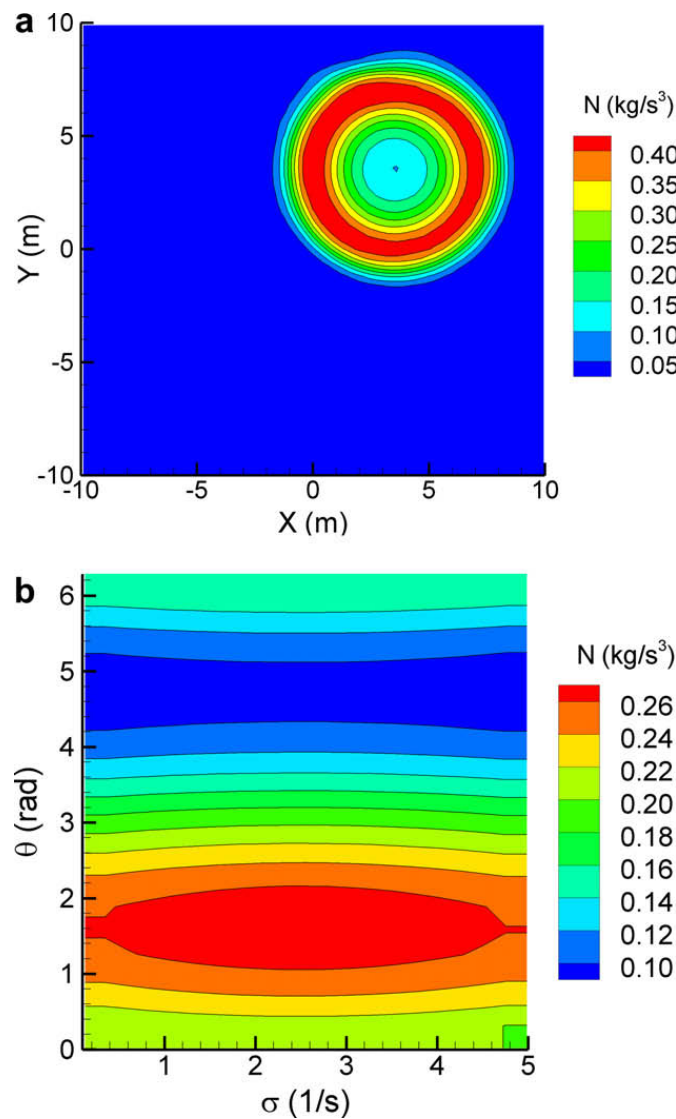


**Fig. 1.** Numerical solution of wave propagation given by (17a) and (17b).  $T = 3.5$  s. Error  $\|N - N^a\|_{\infty} = 3.37 \times 10^{-2}$ , where  $N$  and  $N^a$  are respectively numerical and analytical solution.

$$(\Delta t)_1 = \min_{ij} \left\{ \frac{CFL \cdot \Delta x}{C_{g^{x_{ij,k,l}}}}, \frac{CFL \cdot \Delta y}{C_{g^{y_{ij,k,l}}}}, \frac{CFL \cdot \Delta \sigma}{C_{\sigma_{ij,k,l}}}, \frac{CFL \cdot \Delta \theta}{C_{\theta_{ij,k,l}}} \right\}, \quad (17a)$$

$$(\Delta t)_2 = \min_{ij} \left\{ \frac{CFL \cdot \Delta x}{|U_{ij}| + \sqrt{gH_{ij}}}, \frac{CFL \cdot \Delta y}{|V_{ij}| + \sqrt{gH_{ij}}}, \frac{von \cdot \min(\Delta x^2, \Delta y^2)}{v_{t_{ij}}} \right\}, \quad (17b)$$

$$(\Delta t)_3 = \min_{ij} \left\{ \frac{CFL \cdot \Delta x}{|U_{ij}|}, \frac{CFL \cdot \Delta y}{|V_{ij}|} \right\}, \quad (17c)$$

where CFL and von are constants. The time step for the coupled system is

$$\Delta t = \min\{(\Delta t)_1, (\Delta t)_2, (\Delta t)_3\}. \quad (17d)$$

## 4. Numerical examples

### 4.1. Validation

The numerical methods presented in the previous section and the corresponding computer code are validated using various test problems with analytical solutions. The first test problem is long wave propagation in a uniform current with

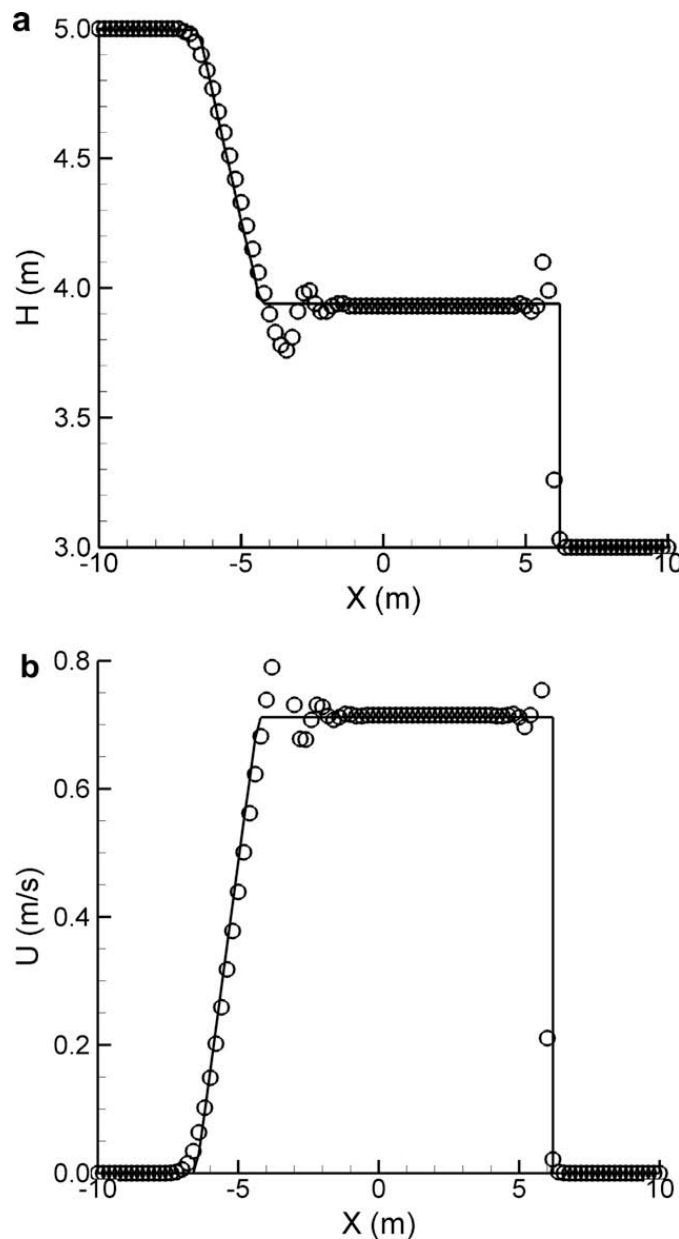


Fig. 2. Solution for surge problem Eqs. (18a) and (18b). T = 2 s. Lines – exact solutions, circles – numerical solutions.

$$U = 1 \text{ m/s}, \quad V = 1 \text{ m/s}, \quad H = 1 \text{ m}, \tag{18a}$$

and the source term given as

$$S = 4a_5N((x-t)^2 + (y-t)^2 - t^2)(x+y-2t-a_1t - C_{gx}(x-t) - C_{gy}(y-t)) + a_6N\left(\frac{1}{1-\exp(-a_6t)} + \frac{1}{\sigma} - 2a_2(\sigma - a_3)\right) + \frac{a_4NC_\theta \cos a_4t}{2 + \sin a_4\theta}. \tag{18b}$$

A solution of Eq. (1) is

$$N = a_7(1 - \exp\{-a_6t\})(2 + \sin a_4\theta) \exp\{-a_2(\sigma - a_3)^2\} \exp\{-a_5((x-t)^2 + (y-t)^2 - a_1t^2)^2\}, \tag{18c}$$

which is a moving circular ring with a diameter increasing with time. Let  $a_1 = 1$ ,  $a_2 = 0.001$ ,  $a_3 = 2.5$ ,  $a_4 = 1$ ,  $a_5 = 0.01$ ,  $a_6 = 0.05$ ,  $a_7 = 1$ ,  $\Delta x, \Delta y = 0.4 \text{ m}$ , and  $\text{CFL} = 0.5$ . The numerical solution is plotted in Fig. 1 with the error given in the figure caption.

The second test problem is a one-dimensional surge-current without viscosity, surface, and bottom friction. The initial condition is

$$x \leq 0: \quad U = 2 \text{ m/s} \quad V = 0 \text{ m/s}, \quad H = 5 \text{ m}, \tag{19a}$$

$$x > 0: \quad U = 2 \text{ m/s}, \quad V = 0 \text{ m/s}, \quad H = 3 \text{ m}. \tag{19b}$$

Letting  $\Delta x = \Delta y = 0.2\text{m}$  and  $\text{CFL} = 0.95$ , the numerical solution is obtained as shown in Fig. 2, together with the corresponding exact solution (e.g., [32]).

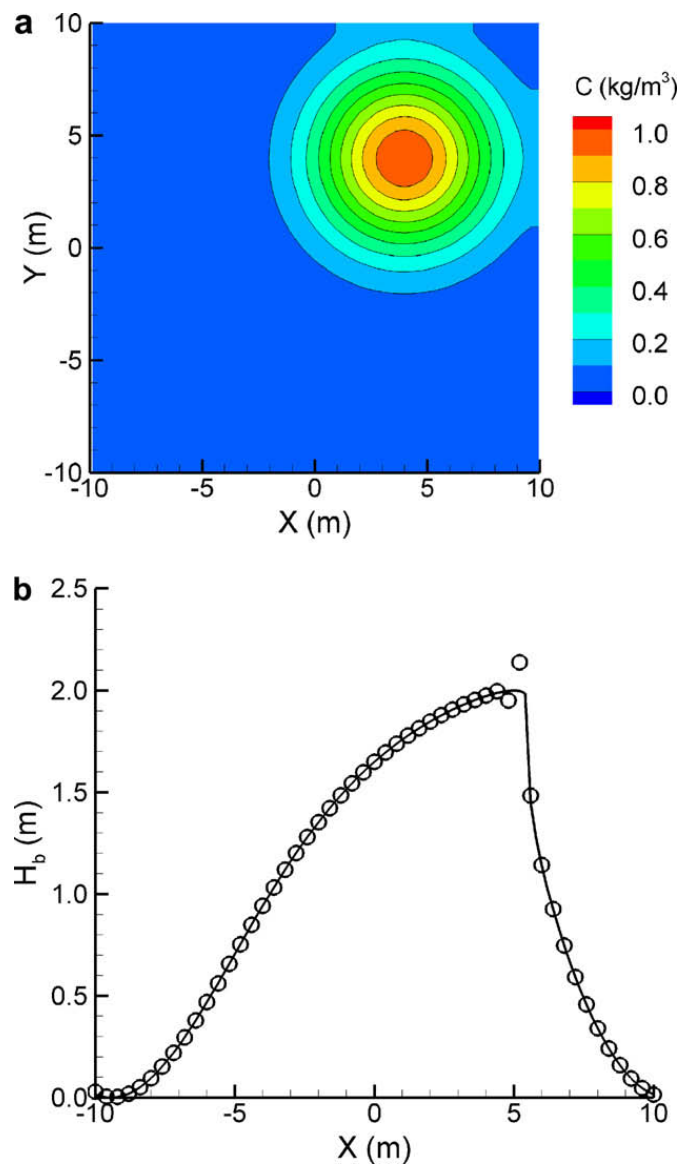


**Fig. 3.** (a) Numerical solution for sediment transport from a point source.  $T = 4 \text{ s}$ . Error  $\|C - C^a\|_\infty = 1.35 \times 10^{-2}$ , where  $C$  and  $C^a$  are respectively numerical and analytical solution. (b) Morphology evolution.  $T = 5 \text{ s}$ . Lines – exact solutions, circles – numerical solutions.

The third test problem is an initial value problem for sediment transport with a point source that has the following solution ([33]):

$$C = \frac{K}{4\pi D_c t} \exp \left[ -\frac{(x - Ut)^2}{4D_c t} - \frac{(x - Vt)^2}{4D_c t} \right]. \quad (20)$$

The point source is initially located at  $(x,y) = (0,0)$ , and  $K = 50$ ,  $U, V = 1$  m/s, and  $D_c = 1$  m<sup>2</sup>/s. With  $\Delta x, \Delta y = 0.4$  m, CFL = 0.95, and von = 0.2, the numerical solution is obtained as shown in Fig. 3a. The last test problem is an initial value problem of one-dimensional seabed evolution from initial elevation

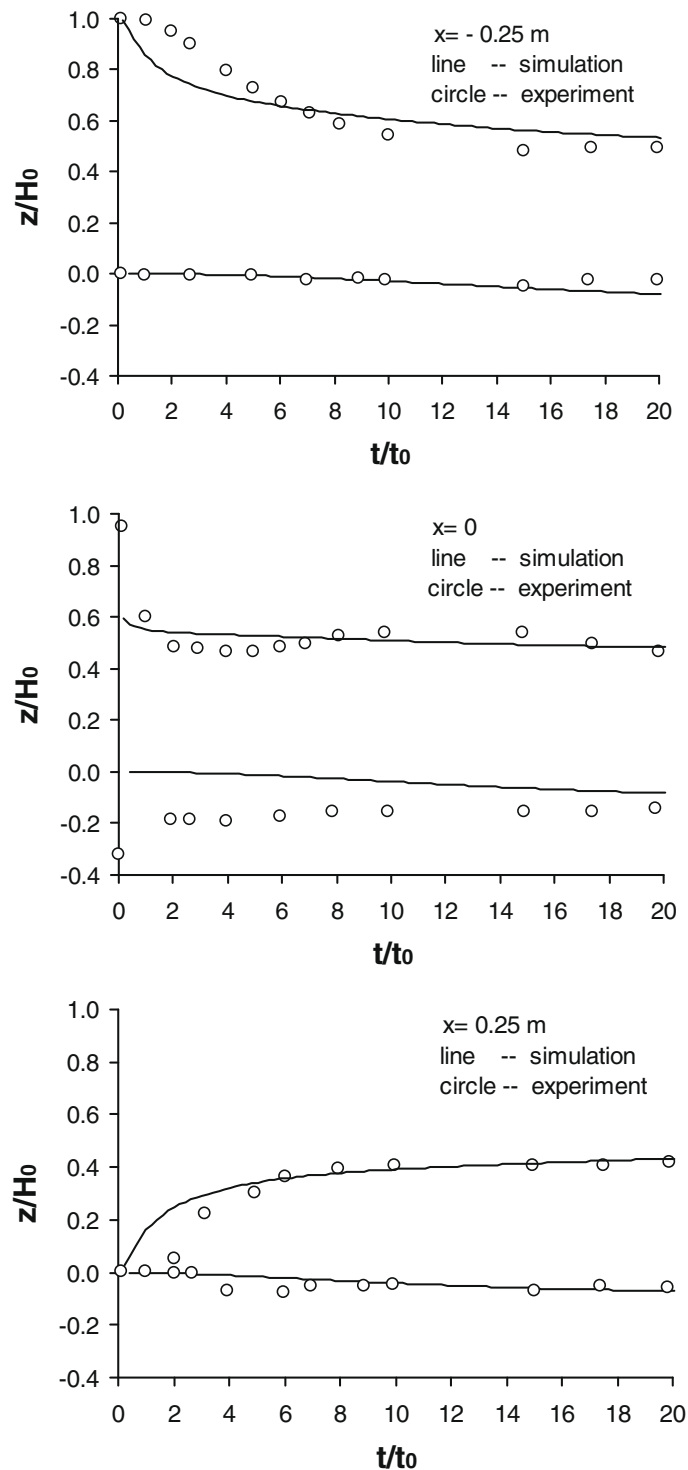


Fig. 4. Solutions for water surface and bed morphology elevations ( $z$ ) of dam-break flow over mobile-bed.

$$H_b = 1 + \cos\left(\frac{\pi x}{10}\right), \tag{21a}$$

with  $BU(U^2 + V^2)^q = 1/H$  in Eq. (12) (e.g., [29]). An exact solution is (e.g., [27,29])

$$H_b = 1 + \cos\left(\frac{\pi}{10}\left(x - \frac{t}{(3 - H_b)^2}\right)\right). \tag{21b}$$

The numerical solution is presented in Fig. 3b with  $\Delta x = 0.2$  m, and CFL=0.95. All of these tests indicate that the numerical methods and the computer code work correctly.

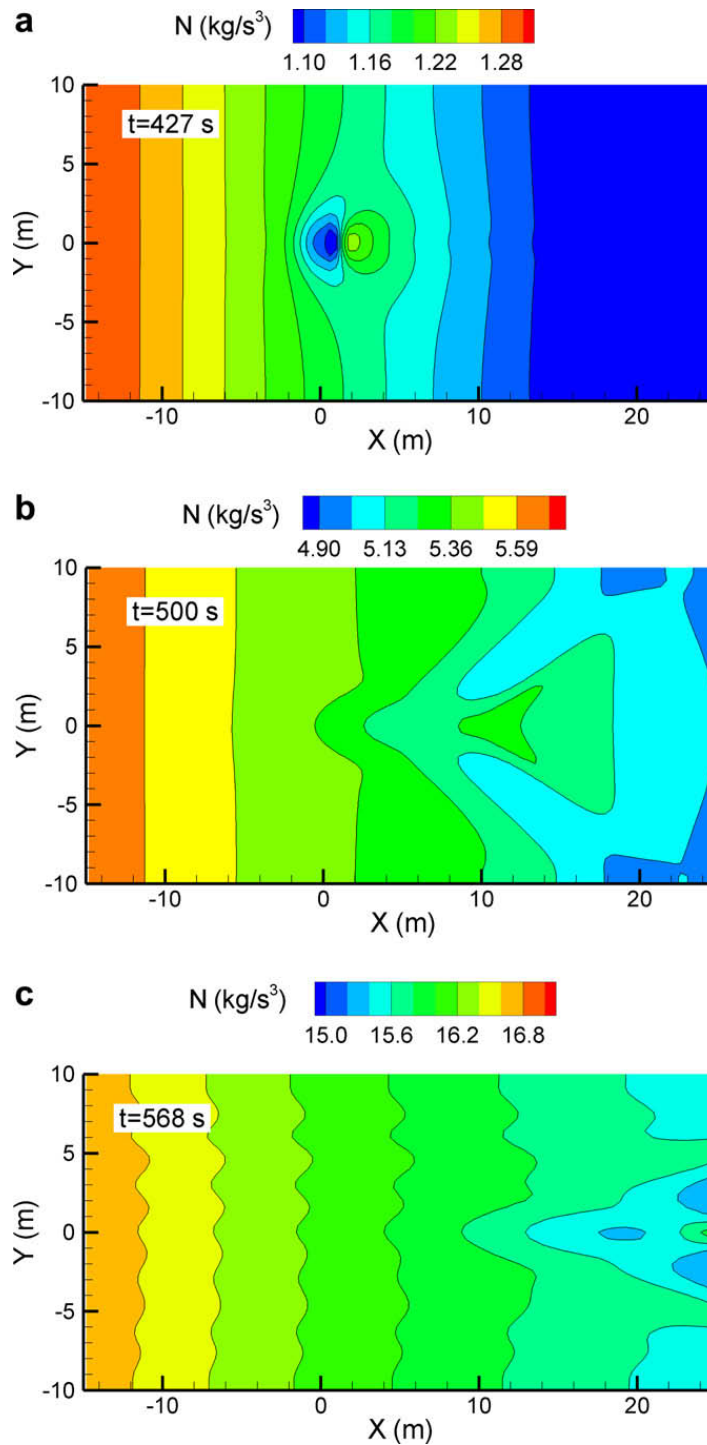


Fig. 5. Solution of wave action for the wave-driven dune problem.

4.2. Applications

The first application represents the interaction between surge and bed morphology in an idealized dam-break experiment over a movable and initially flat bed, as described by Spinewine and Zech [34]. A horizontal glass-walled flume of rectangular cross sectional geometry was used. The initial bed profile featured flat horizontal reaches upstream and downstream of a gate, with a saturated bed of constant thickness. In the upstream reach, a water layer of 0.1 m was retained and released at time 0 s by raising the gate rapidly. The problem is formulated as the following initial value problem:

$$x \leq 0 : U = 0 \text{ m/s}, \quad V = 0 \text{ m/s}, \quad H = 0.1 \text{ m}, \quad H_b = 0 \text{ m}, \tag{22a}$$

$$x > 0 : U = 0 \text{ m/s}, \quad V = 0 \text{ m/s}, \quad H = 0.002 \text{ m}, \quad H_b = 0 \text{ m}. \tag{22b}$$

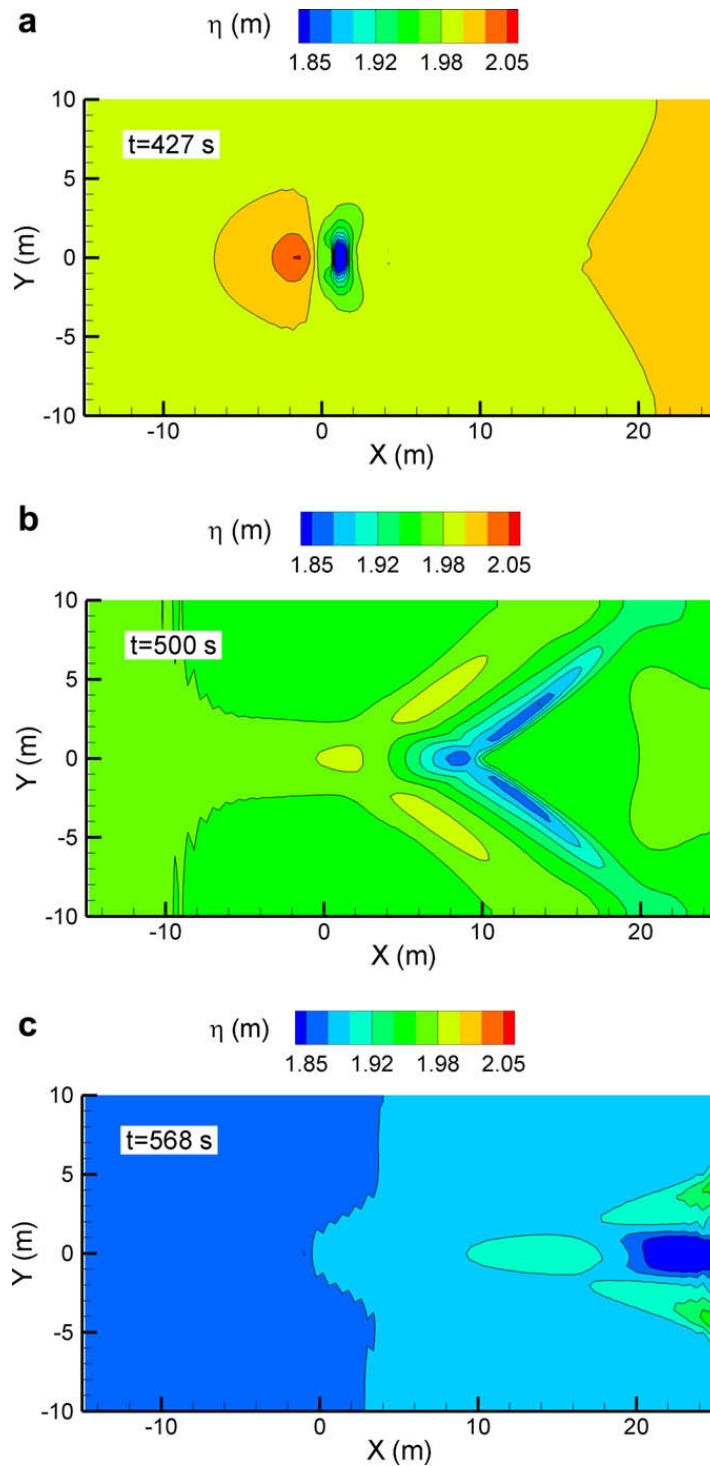


Fig. 6. Solution of current for the wave-driven dune problem.

Here a thin layer of water is given at  $x > 0$  for convenience of computation and the Lax–Friedrich scheme [30] is used for the surge with the following parameters:  $n = 0.025$ ,  $B = 0.1$  1/s,  $\Delta x = 0.05$  m,  $CFL = 0.95$ , and  $\text{von} = 0.5$ .

The numerical solution is obtained as shown in Fig. 4. In the figure,  $H_0 = 0.1$  m,  $t_0 = \sqrt{H_0/g}$ , and numerical solutions and experiment measurements for both water surface and bed elevations are presented at  $x = 0$  (gate location),  $x = -0.25$  m (upstream), and  $x = 0.25$  m (downstream). It is seen that the surface elevation decreases upstream, increases downstream, and remains about the same at the gate. All three locations experience flushing and the bed elevation decreases. The figure shows that there is reasonable agreement between the simulation and the experimental data for both surface and bed elevations. A large difference between simulation and experiment occurs mainly at the initial time at the gate, which is probably attributable to three-dimensional effects that the model does not capture. The degree of agreement between numerical simulation and experimental measurement is about same as that in work of Abderrezzak et al. [35].

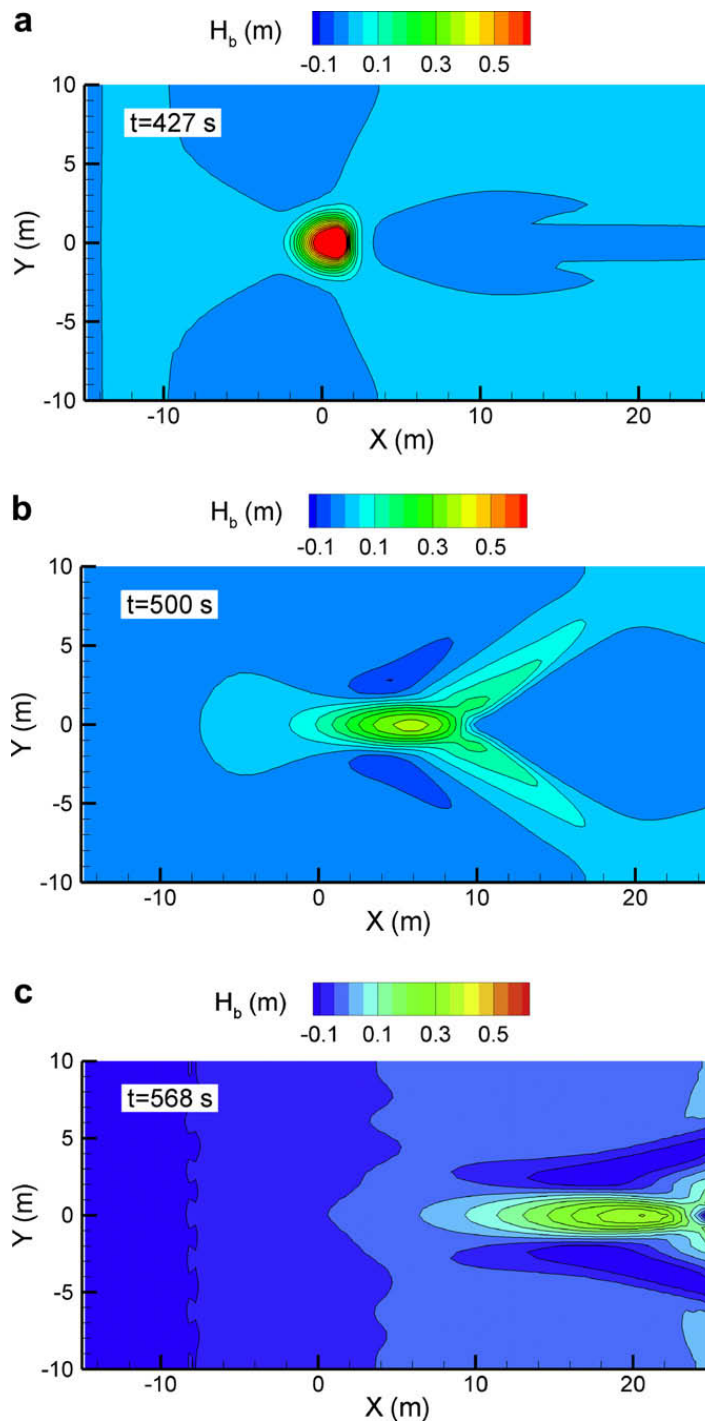


Fig. 7. Solution of morphology for the wave-driven dune problem.

The second application is a short wave-driven flow over a sand dune. The initial conditions for the wave action, the velocity field, and the bottom shape are, respectively

$$N = 0, \quad (23a)$$

$$U = 0, \quad V = 0, \quad H = 2 - \exp\{-0.01(x^2 + y^2)\}, \quad (23b)$$

$$H_b = \exp\{-0.01(x^2 + y^2)\}. \quad (23c)$$

The upstream boundary condition is

$$H = 2 \text{ m}, \quad x = -15 \text{ m}. \quad (23d)$$

The wave action is introduced as a source term in Eq. (1) at the upstream end

$$S = 0.15(1 - \tanh(20 + x - 0.01t)), \quad (23e)$$

which generates waves starting at the upstream end and propagating in the  $x$ -direction:  $n = 0.025$ ,  $\alpha_t = 1$ , and a short wave is considered. In the simulation,  $\Delta x$ ,  $\Delta y = 0.4$  m,  $\Delta \sigma = 0.1$  1/s,  $\Delta \theta = 0.76$  radians, CFL = 0.5, and von = 0.2. Extrapolation is used to update solutions at the boundaries.

The instantaneous solutions at three different moments are given in Figs. 5–7. As shown in Fig. 7, initially ( $t = 427$  s), the shape of the sand dune is changing into a triangle, and low-elevation regions are forming at the upstream region, lateral sides and immediately downstream of the sand dune. At the same time, the sand dune is propagating downstream, and its height gradually decreases. In this process, the sand dune becomes asteroidal ( $t = 500$  s), which is consistent with other simulations (e.g., [16]). The low-elevation regions enlarge and merge, and the elevations at the upstream region and lateral sides of the sand dune become the lowest ( $t = 500$  s, 568 s). Finally, the sand dune is removed by the flow and the final seabed elevation is lower than the initial value throughout the model domain. Fig. 6 shows that surface elevation reaches its highest value in front of the sand dune but forms a dip immediately behind it, and it gradually decreases in all regions. Fig. 5 indicates that wave action takes larger values at the upstream end, and it propagates downstream. It can also be seen from Figs. 5 and 6 that, during the evolution of the sand dune, both the wave field and water surface elevation evolve congruently with the sand dune. Fig. 5 reveals clear traces of bed morphology, which indicate its strong effect on the wave field.

## 5. Concluding remarks

This study presents a framework for synchronically coupling wave, current, sediment transport, and bed morphology as well as preliminary simulation results. The numerical algorithms adopted in the paper lack the high-resolution capability required for rapidly evolving flow like surges, and they could lead to spurious oscillations. Besides, the algorithms have severe restrictions on time step because of their explicit forms. Alternative high-resolution schemes should be developed for the coupled system. More comprehensive validation tests with experimental and field data are needed to test the capability of the proposed coupled framework. Furthermore, in order to provide guidance for coupling actual models (e.g., SWAN) in practical simulations, it would be useful to study strategies for coupling waves, currents, sediment transport, and morphology, that will permit different models to use with different time steps and grid spacing.

## Acknowledgements

The first author is partially supported by PSC-CUNY Research Award. Partial support also came from National Research Council Research Associateship Award. The second author was supported by the Office of Naval Research through the NRL Core project, "Coastal Dynamics in Heterogeneous Sedimentary Environments," (Program Element 61153N). The authors thank Mr. W.E. Roger and Dr. L. Hsu for their valuable advice. Usage of CUNY HPC is acknowledged.

## References

- [1] Kennish MJ. Estuary restoration and maintenance: the national estuary program. CRC Press; 1999.
- [2] Peloquin RA. The Navy ocean modeling and prediction program. From research to operations: an overview. *Oceanography* 1992;5:4–8.
- [3] Blumberg AF, Mellor GL. A description of a three-dimensional coastal ocean circulation model. In: Heaps N, editor. Three dimensional coastal ocean models. American Geophysical Union; 1987. p. 1–16.
- [4] Kara AB, Barron CN, Martin PJ, Smedstad LF, Rhodes RC. Validation of interannual simulations from the 1/8° global Navy Coastal Ocean Model (NCOM). *Ocean Model* 2006;11:376–98.
- [5] Van Dongeren AR, Svendsen IA. Nonlinear and 3D effects in leaky infragravity waves. *Coast Eng* 2000;41:467–96.
- [6] Booij N, Ris RC, Hoithuijsen LH. A third-generation wave model for coastal regions, I. Model description and validation. *J Geophys Res* 1999;104:7649–66.
- [7] Tolman HL. 1991: A third-generation model for wind waves on slowly varying, unsteady and inhomogeneous depths and currents. *J Phys Oceanogr* 1991;21:782–97.
- [8] Papanicolaou AN, Elhakeem M, Krallis G, Prakash S, Edinger J. The morphodynamic modeling of tidal sand waves on the shoreface. *ASCE J Hydr Eng* 2008;134:1–14.
- [9] Tonnon PK, van Rijn LC, Walstra DJR. The morphodynamic modeling of tidal sand waves on the shoreface. *Coast Eng* 2007;54:279–96.
- [10] Xie L, Pietrafesa LJ, Wu K. A numerical study of wave-current interaction through surface and bottom stresses: coastal ocean response to Hurricane Fran of 1996. *J Geophys Res C2* 2003;108:31–18.
- [11] Liang B, Li H, Lee D. Numerical study of three-dimensional sediment transport in waves and currents. *Ocean Eng* 2007;34:1569–83.

- [12] Pandoe WW, Edge BL. Case study for a cohesive sediment transport model for Matagorda Bay, Texas, with coupled ADCIRC 2D-transport and SWAN wave models. *ASCE J Hydr Eng* 2008;134:303–14.
- [13] Rogers BD, Borthwick AGL, Taylor PH. Godunov-type adaptive grid model of wave–current interaction at cusped beaches. *Int J Numer Meth Fluids* 2004;46:569–606.
- [14] Murillo J, Burguete J, Brufau P, Garcia-Navarro P. Coupling between shallow water and solute flow equations: analysis and management of source terms in 2D. *Int J Numer Meth Fluids* 2005;49:267–99.
- [15] Hudson J, Sweby PK. Formulations for numerically approximating hyperbolic systems governing sediment transport. *J Sci Comput* 2003;19:225–52.
- [16] Hudson J, Sweby PK. A high-resolution scheme for the equations governing 2D bed-load sediment transport. *J Numer Meth Fluids* 2005;47:1085–91.
- [17] Rosatti G, Fraccarollo L. A well-balanced approach for flows over mobile-bed with high sediment-transport. *J Comput Phys* 2006;220:312–38.
- [18] Rogers BD, Borthwick AGL, Taylor PH. Mathematical balancing of flux gradient and source terms prior to using Roe's approximate Riemann solver. *J Comput Phys* 2003;192:422–51.
- [19] Bermudez A, Vazquez ME. Upwind methods for hyperbolic conservation laws with source terms. *Comput Fluids* 1994;23:1049–71.
- [20] Mei CC. *Applied dynamics of ocean waves*. John Wiley & Sons; 1983.
- [21] Rogers WE, Kaihatu JM, Petit HAH, Booij N, Holthuijsen LH. Diffusion reduction in an arbitrary scale third generation wind wave model. *Ocean Eng* 2002;29:1357–90.
- [22] Wu W. Depth-averaged two-dimensional numerical modeling of unsteady flow and nonuniform sediment transport in open channels. *J Hydraul Eng* 2004;130:1013–24.
- [23] Soulis JV. A fully coupled numerical technique for 2D bed morphology calculation. *Int J Numer Meth Fluids* 2002;38:71–98.
- [24] Xie L, Wu K, Pietrafesa L, Zhang C. A numerical study of wave–current interaction through surface and bottom stress: wind-driven circulation in the South Atlantic Bight under uniform winds. *J Geophys Res* 2001;106:16841–55.
- [25] Svendsen A, Haas K, Zhao Q. Qusia-3D nearshore circulation model. SHORECIRC, version 2.0. U. of Delaware: Center for Applied Coastal Research.
- [26] WAMDI Group. The WAM model: a third generation ocean wave prediction model. *J Phys Oceanogr* 18(1988):1775–1810.
- [27] Exner FM. *Über die Wechselwirkung zwischen Wasser und Geschiebe in Flüssen*. Sitzungsber Akad Wiss Wien Math Naturwiss Kl Abt 2A 1925;134:165–80.
- [28] Sleath JFA. *Sea bed mechanics*. New York: John Wiley & Sons; 1984.
- [29] Kubatko EJ, Westerink JJ, Dawson Clint. An unstructured grid morphodynamics model with a discontinuous Galerkin method for bed evolution. *Ocean Model* 2006;15:71–89.
- [30] Lax PD. Weak solutions of nonlinear hyperbolic equations and their numerical computation. *Commun Pure Appl Math* 1954;7:159–93.
- [31] McCormack RW. The effect of viscosity in hypervelocity impact cratering. *AIAA Paper* 1969:69–354.
- [32] Tang HS, Huang D. A second-order accurate capturing scheme for 1D inviscid flows of gas and water with vacuum zones. *J Comput Phys* 1996;128:301–18.
- [33] Sankaranarayanan S, Shankar NJ, Cheong HF. Three-dimensional finite difference model for transport of conservative pollutants. *Ocean Eng* 1998;25:425–42.
- [34] Spinewine B, Zech Y. Dam-break waves over movable beds: a flat bed test case. In: Paper presented at the 2nd IMPACT workshop, Statkraft Grøner, Mo-i-Rana, 12–13 September 2002. Available at [www.impact-project.net](http://www.impact-project.net).
- [35] El K, Abderrezzak K, Paquier A, Gay B. One-dimensional numerical modelling of dam-break waves over movable beds: application to experimental and field cases. *Environ Fluid Mech* 2008;8:169–98.